Systems/Circuits

Dissociation of LFP Power and Tuning in the Frontal Cortex during Memory

Charles D. Holmes,[1,2] Charalampos Papadimitriou,[1] and Lawrence H. Snyder[1,2]

[1]Department of Neuroscience, Washington University in St. Louis, St. Louis, Missouri 63110 and [2]Department of Biomedical Engineering, Washington University School of Medicine, St. Louis, Missouri 63130

Working memory, the ability to maintain and manipulate information in the brain, is critical for cognition. During the memory period of spatial memory tasks, neurons in the prefrontal cortex code for memorized locations via persistent, spatially tuned increases in activity. Local field potentials (LFPs) are understood to reflect summed synaptic activity of local neuron populations and may offer a window into network-level processing. We recorded LFPs from areas 8A and 9/46 while two male cynomolgus macaques (*Macaca fascicularis*) performed a long duration (5.1–15.6 s) memory-guided saccade task. Greater than ~16 Hz, LFP power was contralaterally tuned throughout the memory period. Yet power for both contralateral and ipsilateral targets fell gradually after the first second of the memory period, dropping below baseline after a few seconds. Our results dissociate absolute LFP power from mnemonic tuning and are consistent with modeling work that suggests that decreasing synchronization within a network may improve the stability of memory coding.

Key words: frontal eye fields; local field potential; macaque; prefrontal cortex; working memory

Significance Statement

The frontal cortex is an important site for working memory. There, individual neurons reflect memorized information with selective increases in activity, but how collections of neurons work together to achieve memory is not well understood. In this work, we examined rhythmic electrical activity surrounding these neurons, which may reflect the operation of recurrent circuitry that could underlie memory. This rhythmic activity was spatially tuned with respect to memorized locations as long as memory was tested (~7.5 s). Surprisingly, however, the overall magnitude of rhythmic activity decreased steadily over this period, dropping below baseline levels after a few seconds. These findings suggest that collections of neurons may actively desynchronize to promote stability in memory circuitry.

Introduction

Working memory is the cognitive function that underlies the short-term storage, manipulation, and utilization of information. A large body of evidence demonstrates that neural activity in the prefrontal cortex is a correlate of working memory. Prefrontal neurons increase their firing rate throughout the delay interval of memory tasks (Funahashi et al., 1989; Wimmer et al., 2014). Individual neurons exhibit tuning, i.e., different memoranda systematically elicit different levels of activity. For spatial memoranda, memory-period firing rate is typically a bell-shaped function of the memorandum's angle in gaze-centered space. Modeling suggests that this tuned mnemonic activity may be sustained by recurrent feedback (Compte et al., 2000) and this claim has been supported by experimental evidence (Wimmer et al., 2014).

Although the study of individual neurons reveals that neurons code memorized information during working memory, it does not provide direct information about how networks of neurons interact and work together. Recurrent feedback may lead to networks of neurons synchronizing (Buzsáki and Wang, 2012). However, neuronal spiking is stochastic and synchronization is only partial, and thus documenting synchronization between pairs of neurons requires a large amount of data (Cohen and Kohn, 2011). A lower frequency electrophysiological signal, the local field potential (LFP), is thought to reflect a summation of transmembrane currents, largely from dendritic processes of local ensembles of neurons (Buzsáki et al., 2012). If this formulation is correct, then the amplitude of the LFP reflects the degree of

Received Dec. 25, 2017; revised July 18, 2018; accepted July 20, 2018.

Author contributions: C.D.H. and L.H.S. wrote the first draft of the paper; C.D.H. and L.H.S. edited the paper; C.P. and L.H.S. designed research; C.D.H., C.P., and L.H.S. performed research; C.D.H., C.P., and L.H.S. analyzed data; C.D.H. and L.H.S. wrote the paper.

We thank B. Acland, E. Mooshagian, J. Li, K. Conen, and L. Katz for helpful discussion and feedback regarding this work, and J. Tucker for helping with technical issues.

This work is supported by National Eye Institute (grant number R01-EY012135 to L.H.S.), National Institute of Mental Health (grant number 5F31MH094076 to C.P.), and National Science Foundation (grant number T32-NS073547 to C.D.H and C.P.).

The authors declare no competing financial interests.

Correspondence should be addressed to Charles D. Holmes, 660 South Euclid Avenue, Box 8108, St. Louis, MO 63110. E-mail: holmes@eye-hand.wustl.edu.

DOI:10.1523/JNEUROSCI.3629-17.2018

 0270-6474/18/388177-10$15.00/0

synchronicity in these currents. Therefore, the study of LFPs may offer a window into network-level synchronization and, more generally, network-level processing in the prefrontal cortex.

Previous work has shown that holding memories for a few seconds is associated with evoked LFP responses in the cortex (Monosov et al., 2008) and power modulations in theta (Jensen and Tesche, 2002; Hsieh et al., 2011), alpha (Jensen et al., 2002; Hsieh et al., 2011) beta (Roberts et al., 2013; Kornblith et al., 2016), and gamma frequencies (Pesaran et al., 2002; Howard et al., 2003; Roberts et al., 2013; Kornblith et al., 2016). However, many of these studies use memory durations of a few seconds or less. It is unknown whether such LFP responses persist for longer durations, and whether they might evolve with time. Such results would have implications for memory network dynamics and further constrain theories of how cortex maintains information.

For this work, we hypothesized that memory maintenance is associated with a sustained increase in neural synchronization, which leads to synchronized dendritic currents, which manifests as elevated LFP power. We further hypothesized that the elevation in LFP power would be spatially tuned and would persist for as long as the memory was maintained. To test this, we recorded LFPs in prefrontal cortex, specifically areas 8A and 9/46 (Petrides et al., 2012), during a memory-guided saccade task. We used long memory periods (5.1–15.6 s) to better distinguish transient from sustained effects. We found that LFP power $>\sim$16 Hz showed a bias for contralateral targets (spatial tuning) that was sustained for the entire memory period. In contrast, absolute power increased in response to stimulus presentation but then fell, dropping below baseline after $\sim$1–5 s. These results suggest that frontal memory circuits synchronize in response to stimulus presentation and/or memory encoding, and then gradually desynchronize to below the baseline level over the course of a long memory period. This network desynchronization may promote memory state stability while the sustained contralateral bias may be a correlate of neuronal memory tuning.

Materials and Methods

Experimental design. Two male cynomolgus macaques (*Macaca fascicularis*; C and W) participated in the study. All procedures conformed to the *Guide for the Care and Use of Laboratory Animals* and were approved by the Washington University Institutional Animal Care and Use Committee. Each animal was fit with a head post and a recording chamber. The recording chamber was located over the left hemisphere arcuate and principal sulci to allow access to areas 8A and 9/46, respectively.

During experiments, the animals sat in customized primate chairs and were placed in a completely dark room. Visual stimuli were back projected onto a screen in front of the animal using a CRT video projector. Eye position was monitored with an infrared video eye-tracking system (ISCAN).

Each trial began with the animal gazing within 3.3 degrees of visual angle (dva) of a central fixation point for 1.5 s. A peripheral target then appeared for 300 ms, whose location the animal needed to remember to properly perform the task. Each target was at a random location on an invisible circle centered on the fixation point with a radius between 10 and 15 dva. The radius of the circle was fixed for each individual recording session. Trials with memory periods of 5.1, 7.6, or 15.1 s were interleaved. There was an additional 0–0.5 s of random delay intended to decrease predictability. Trials were aborted if the animal broke fixation during either the fixation or memory periods. The disappearance of the fixation point cued a saccade to the remembered location. The trial was classified as an error and immediately aborted if the saccade landed very far from the target, i.e., outside of a 16×20 dva window centered around the target location, corresponding to a directional error $\geq\sim$45 degrees of arc (deg). If the saccade landed within 5.5 dva of the target location, a reward was immediately delivered, encouraging accurate mnemonic behavior. For intermediate saccade landing points, the trial was not aborted but no immediate reward was delivered. The target reappeared after another 300 ms. Once the animal made a saccade to within 3.5 dva of the now visible target, a final reward was delivered, and the trial ended. Rarely, the animal failed to make this final saccade and the trial was aborted. Thus, the animal would receive up to two rewards per trial, depending on its mnemonic accuracy.

During the memory period, but before the saccade, the animal received two juice rewards: one 7.8 s after target onset and another 12.8 s after target onset (215 recording sites). These rewards encouraged the animal to maintain fixation over long (>7.5 s) intervals. For 20 sites in Monkey C, rewards were delivered at 6.3, 10.3, and 12.3 s after target onset. For 27 sites in Monkey W, rewards were delivered every 2.5 s during memory. Results from these 47 sites were similar to the results from the 215 sites that form the basis of this report.

Electrophysiological recordings. During each recording session, we inserted 1–4 tungsten microelectrodes (FHC or AlphaOmega; 0.2–2 MΩ) into the prefrontal cortex. After each session, all electrodes were removed. We recorded LFPs from 215 sites using our standard reward schedule, 132 from area 8A (90 from Monkey C, 42 from Monkey W) and 83 from area 9/46 (42 from Monkey C, 41 from Monkey W), that were all within 2 mm of a neuron tuned during some portion of the memory period. Saccades could be evoked from the area 8A sites, but not from the 9/46 sites, using 50 μA of current or less. The results of the unit recording will be presented in a separate report. Field potentials were amplified (FHC), filtered (0.075–300 Hz bandpass and 60 Hz notch), and sampled at 1.56 kHz. Results were similar across both areas (see Results) and so we combined data across areas to improve statistical power.

Signal analysis. We estimated the task-evoked component of the LFP by averaging LFPs across trials and then across sites. Data time series were aligned to stimulus presentation before averaging.

We estimated LFP power spectral densities using a multitaper method with four Slepian tapers. The time-half-bandwidth product was set to 2.5 so that a 625 ms window and a 1250 ms window provided frequency resolutions of $\pm$4 and $\pm$2 Hz, respectively. To produce a spectrum, we computed power spectral density for frequencies from 4 to 128 Hz in 2 Hz steps. For each taper, w_k, we estimated the spectrum, $X_k(f)$, as follows:

$$X_k(f) = \sum_{t=1}^{N} w_k(t)\, x(t) e^{-2\pi jft},$$

where x is the signal of length N, j is the imaginary unit ($\sqrt{-1}$), and f and t are frequency and time indices, respectively. We used an adaptive algorithm to compute a weighted average of the spectrum magnitudes (Percival and Walden, 1993). We normalized the average by the sampling rate to obtain the power spectral density estimate. For most of our presented data, except where noted, we show results from the 625 ms window analysis, to maintain a high temporal resolution.

To examine how spectra evolve over time, we computed power spectrograms with 625 ms windows and 156.25 ms time steps, i.e., one-fourth the length of the window. We computed percentage modulation from baseline by dividing the spectrum at each time point by the mean baseline spectrum and then averaging across sites.

From the spectrograms, we estimated power density spectra over an interval of interest by averaging across time points. We averaged the results obtained from each 625 ms window completely within the larger interval. This allowed us to maintain the same frequency resolution across intervals >625 ms. The mean power density spectrum of each site was normalized by mean broadband power (4–128 Hz) during the baseline interval (1.5–0 s before stimulus onset) before averaging across sites. We excluded data in the first 2 s after stimulus onset to avoid stimulus-driven transients and after 7.8 s to avoid reward-related transients (see Results).

From the spectrograms, we estimated band-limited power by summing the power spectral density within a band of interest. The bands of interest were octave-width bands from 4 to 128 Hz, i.e., 4–8 Hz (theta band), 8–16 Hz (alpha band), etc. For theta band, we estimated spectral data with 1250 ms windows to ensure that our frequency resolution remained within the band ($\pm$2 Hz). For all other bands, we used spectral

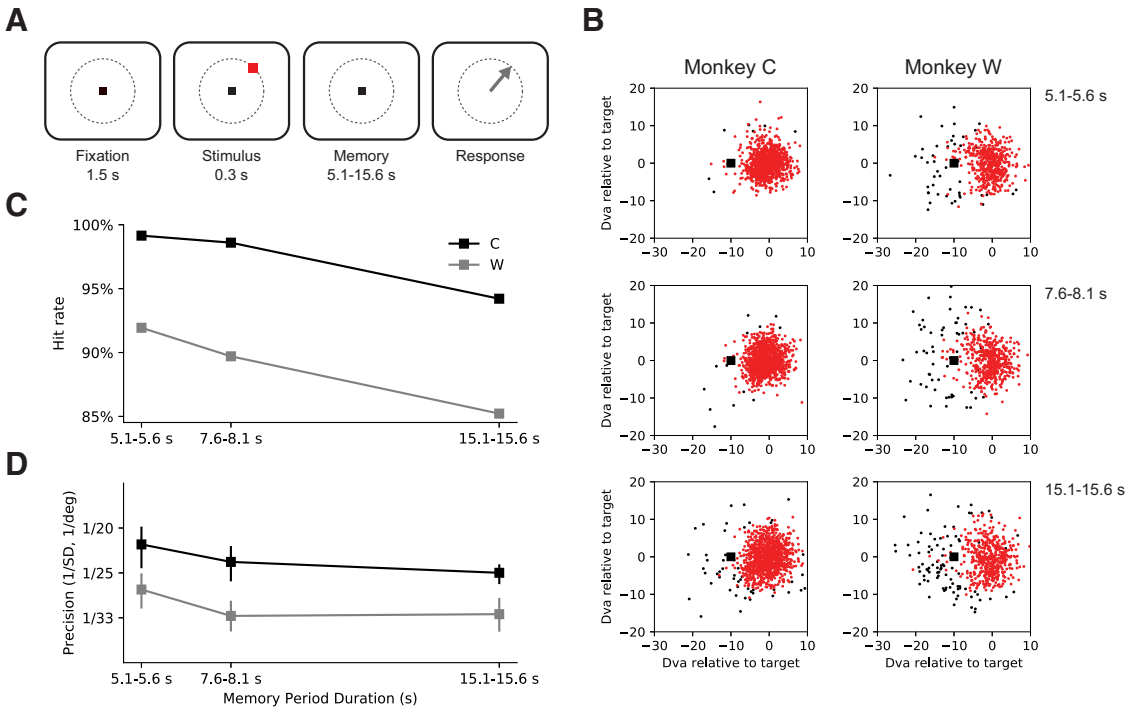

Figure 1. Memory-guided saccade task. ***A***, The subject began each trial with 1.5 s of fixation at a central point (black square). Then, a peripheral target (red square) appeared for 300 ms at a random location about a circle (dotted line; invisible to the subject). Next, the target disappeared, and the subject maintained fixation for 5.1, 7.6, or 15.6 s, plus an additional 0–0.5 s of random duration. Finally, the fixation point disappeared, signaling the subject to make an eye movement (arrow) to the remembered target location. ***B***, Distance of eye positions from the memory target for Monkeys C and W after a memory-guided saccadic response and just before the target reappeared. Data are separated by the trial memory period duration. Data are rotationally aligned about the fixation point (black square) by the location of the memory target. Red points indicate saccades that landed within 8 dva horizontally and 10 dva vertically (before rotational alignment) of the memory target, i.e., successful saccades. Black points indicate the eye positions at the end of error trials. In some trials, animals land within the 16 by 20 dva window but move out of it before the target reappears, resulting in red points far from the target. Only data from trials with memory target eccentricities of 10 deg are shown. ***C***, ***D***, Metrics of memory-guided behavior over time for Monkeys C (black) and W (gray). The hit rate (i.e., percentage of successful saccades) and the reliability of saccade endpoints (measured as 1/SD of the saccadic error, or "saccade precision") decreased with longer memory periods. Saccade precision is plotted with error bars showing 95% bootstrapped CIs. Note that, for normally distributed data, 95% confidence limits are ~2 SEM, so that these error bars are twice as large as conventional error bars.

data estimated with 625 ms windows. We expressed band-limited power as percentage modulation from baseline (average power 1.5–0 s before stimulus onset). We quantified trends in absolute power by fitting a line as a function of time. As with power spectra estimates, data 0–2 s and beyond 7.8 s after stimulus onset were excluded from the fits. Slope significance was assessed with a two-sided t test.

We estimated tuning of LFP power for each site with a von Mises model. Power was estimated for each trial within a frequency band and time interval of interest. These data were then fit to a von Mises function of target direction. The 0 deg direction was defined to be horizontal and to the right (contralateral to the recorded hemisphere) and positive angles proceeded counterclockwise. We fit the power of each trial as a function of target angle, θ, with the following function:

$$f(\theta) = Ae^{\kappa\cos(\theta-\mu)} + b.$$

We fit the four parameters, A (amplitude), κ (spread), μ (preferred direction), and b (offset), using gradient descent with a mean-squared-error cost function. For fits with negative κ, we swapped the sign of κ to be positive and incremented μ by 180 deg. We quantify tuning selectivity as the full-width at half-maximum (FWHM), which can be analytically derived from the spread parameter), κ by the following:

$$FWHM = 2\cos^{-1}\left(\frac{1}{\mathrm{k}}\ln(\cosh(\mathrm{k}))\right).$$

We assessed clustering at the population level by first assigning a unit vector to each LFP site. The unit vectors were averaged across sites to produce a population average preferred direction.

Statistical methods. When we report a statistical value, such as a mean, we typically report the 95% confidence interval (CI) as our measure of statistical uncertainty. CIs are estimated with a bias-corrected and accelerated bootstrap method (DiCiccio and Efron, 1996). Briefly, the data are resampled, with replacement, and averaged 10,000 times to produce a distribution of the statistic. Without bias-correction or acceleration, the CI would range from the 2.5th to the 97.5th percentile of distribution. Bias-correction and acceleration adjust these percentiles for bias and skewness in the distribution. The bounds of the 95% CI are delineations of a $p < 0.05$ test and would be equal to ~2 SEM, were the data normally distributed.

When we estimate the preferred directions of LFP power, we assessed fit significance with an F test, comparing the von Mises model to a zero-slope line model. We tested for clustering of preferred directions across the population with Rayleigh's z test (Zar, 1974). Briefly, this test aims to reject the null hypothesis that the distribution of preferred directions is uniform. We also tested for a laterality bias with a binomial test.

Results

We studied the synchronization of neuronal networks in the frontal cortex as a step toward characterizing circuit-level processing of working memory. Specifically, we examined whether local synchronization reflects memorized information. In our experiments, two male cynomolgus macaques (*Macaca fascicularis*), C and W, performed a memory-guided saccade task (Fig. 1*A*). A peripheral target appeared for 300 ms as the animal fixated a central point. A memory period of 5.1–5.6, 7.6–8.1, or 15.1–15.6 s followed, after which the fixation point disappeared and the animal made a saccade to the remembered target location (Fig. 1*B*). Animals received midtrial rewards during the memory

period, 7.5 and 12.5 s after stimulus offset, to encourage them to stay on task. Monkeys C and W broke fixation during the memory period in 17.3% and 15.6% of trials, respectively, resulting in those trials being aborted. After the memory period, the animals were cued to saccade to the target. Errors, including grossly inaccurate saccade, i.e., off by ≧∼45 deg, or failure to saccade to the target after it reappeared, occurred in 2.7% and 11.1% of non-aborted trials for Monkeys C and W, respectively. Of the remaining non-aborted trials, the saccadic angular precision, i.e., 1/SD, was 1/23 deg^{-1} [bootstrap 95% CI (1/25 $^{-1}$, 1/22 deg^{-1})] and 1/31 deg^{-1} [bootstrap 95% CI (1/33 deg^{-1}, 1/29 deg^{-1})] for Monkeys C and W, respectively. Not surprisingly, performance of memory guided behavior weakened with longer delay intervals. Both the percentage of successful trials (hit rate) and saccade precision decreased with memory period duration (Figs. 1*C*,*D*).

We recorded LFPs at 132 sites on the anterior bank of the arcuate sulcus, corresponding to area 8A, and 83 sites from the posterior portion of the principal sulcus, corresponding to area 9/46 (Fig. 2; Petrides et al., 2012). We performed all of the following analyses separately for each area and found that results were similar and conclusions were identical. Given this, we combined data across areas to improve statistical power.

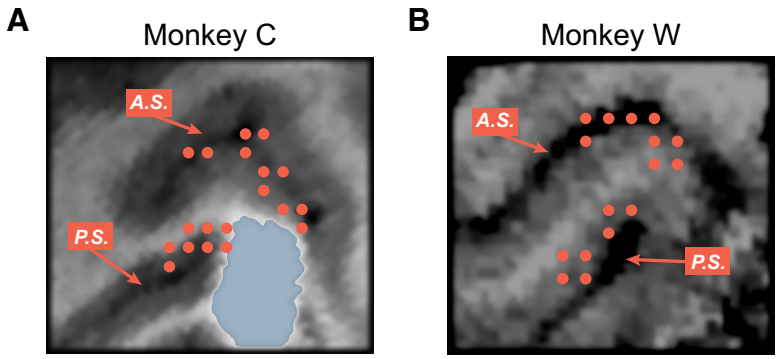

Figure 2. Recording locations. LFP recording locations for Monkeys C (***A***) and W (***B***). Recording locations (red dots) are projected onto a representative anatomical MR image. Electrodes were inserted orthogonally to the plane of these images. LFPs were recorded from area 8A near the arcuate sulcus (A.S.) and from area 9/46 near the principal sulcus (P.S.). The blue highlighted region in Monkey C's image marks an MR-lucent manganese injection, used to verify recording site location.

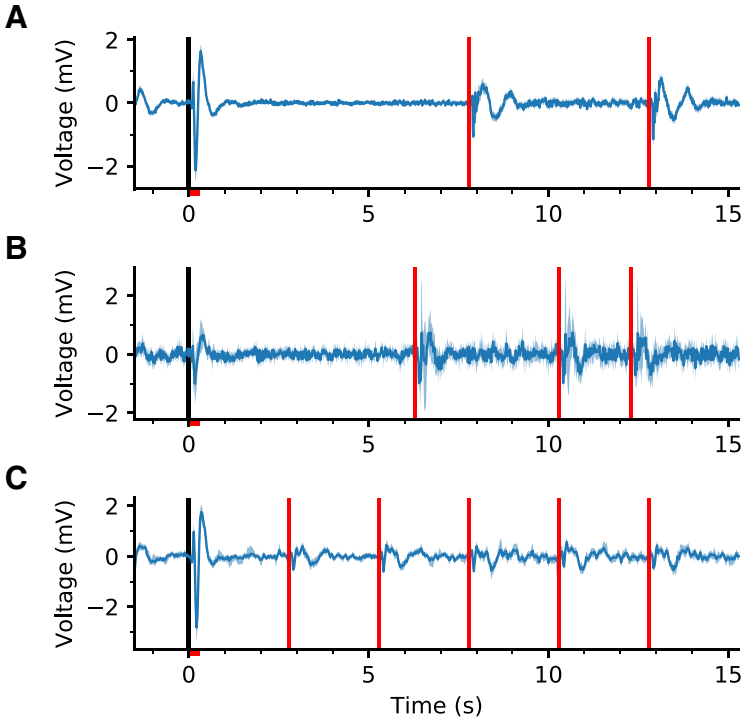

Figure 3. Evoked LFPs. ***A***, The population-averaged evoked LFP (215 sites) shows a transient response to stimulus presentation (0 – 0.3 s; red horizontal bar in *x*-axis) and to reward delivery (7.8 and 12.8 s after the stimulus onset; red vertical lines), but exhibits no sustained memory response. ***B***, The average evoked LFP with rewards at 6.3, 10.3, and 12.3 s after stimulus onset exhibits responses immediately after those rewards (20 sites from Monkey C). ***C***, The average evoked LFP with rewards every 2.5 s exhibits responses immediately after those rewards (27 sites from Monkey W). In all plots, the solid trace depicts the mean and the shaded region depicts the bootstrapped 95% CI. The data are plotted for the fixation (before 0 s), stimulus (0 – 0.3 s), and memory periods (0.3–15.3 s poststimulus onset). All trials contribute data from −1.5 to +5.3 s of stimulus onset. Trials with memory periods of ∼7.5 and ∼15 s contribute data from 5.3 to 7.8 s, whereas only ∼15 s trials contribute data from 7.8 to 15 s.

Evoked LFPs reflect the stimulus and rewards

We first asked whether the memory task elicited an evoked LFP response. We estimated the task-evoked portion of the LFP by averaging LFPs across trials. Signal components that are not phase-locked with task events will average to a value that approaches zero as the number of trials increases, leaving only phase-locked components. There was a stimulus-related response that disappeared within several hundred milliseconds of the stimulus offset, and no sustained response (Fig. 3*A*). For most of the memory period, the LFP voltage was at baseline. Thus, the evoked LFP was unaffected by memory beyond ∼1 s.

There were two transient responses that were not related to memory, but instead were associated with within-trial reward delivery. These responses occurred immediately after midtrial rewards at 7.5 and 12.5 s into the memory period. We verified that the responses were coupled to rewards by changing the number and delivery times of midtrial rewards in a pair of smaller datasets. We collected 20 sites from Monkey C with rewards at 6, 10, and 12 s into the memory period (Fig. 3*B*) and 27 sites from Monkey W with rewards after every 2.5 s of memory (Fig. 3*C*). Responses consistently occurred after reward delivery, supporting the notion that they were reward-evoked. Our design did not allow us to assess whether this response reflects reward coding, a motor response related to reward consumption or an electrical artifact. To avoid potential confounds, although we show a full 15 s of data in subsequent figures, we restrict our analysis and conclusions to the interval before the first midtrial reward, i.e., the 7.8 s after stimulus onset.

LFP power decreases throughout the memory period

Mnemonic processing may affect the variance of the LFP rather than its magnitude. To test this, we examined LFP power spectral

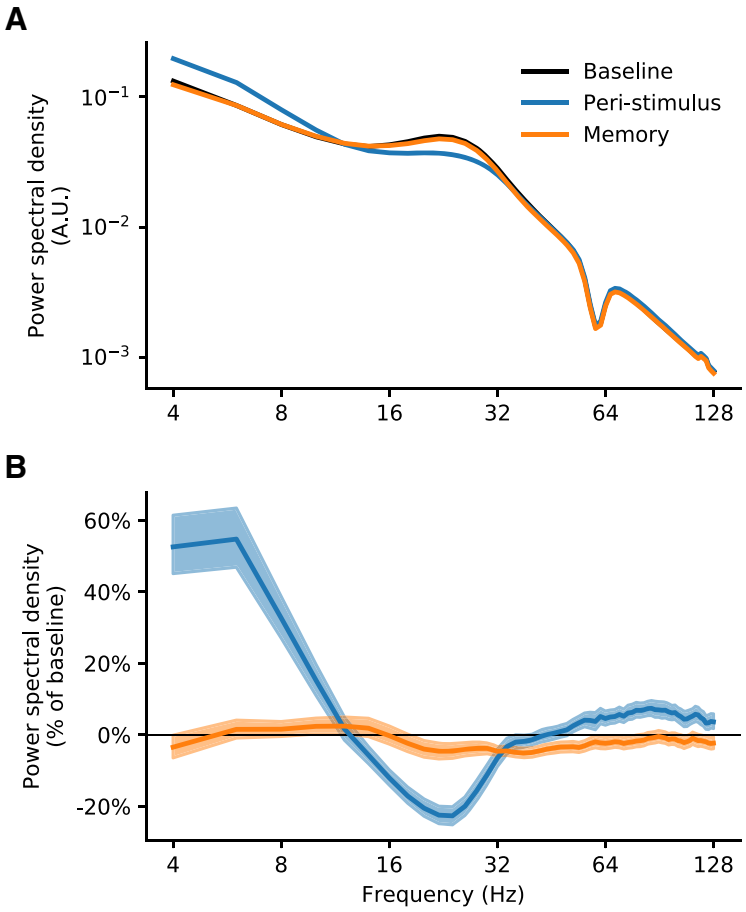

Figure 4. LFP power spectral density. ***A***, The mean power spectral densities (4–128 Hz in 2 Hz steps) from baseline (1.5–0 s before the stimulus; black), a peristimulus interval (0–1 s after stimulus onset; blue), and the memory interval (2–7.8 s after stimulus onset; orange) were all similar with subtle, frequency-specific differences. The spectrum of each site was normalized by mean broadband power (summed across 4–128 Hz) during baseline before averaging across sites. The dip at 60 Hz is caused by a 60 Hz notch filter in the amplifier. ***B***, Mean percentage difference from baseline of the power spectral density for the peristimulus (blue) and memory interval (orange). The solid traces depict mean and the shading depicts the bootstrapped 95% CI (approximately twice the size of conventional error bars). Power in the theta (4–8 Hz) and alpha bands (8–16 Hz) was greater for the peristimulus interval, whereas baseline and memory power were similar. Beta-band (16–32 Hz) power was greatest for baseline, followed by memory and then the peristimulus interval. Gamma-(32–64 Hz) and high-gamma-band power (64–128 Hz) was greatest for the peristimulus interval, followed by baseline and then memory.

density, which captures how signal variance is spread across frequencies. This was computed as a function of frequency and averaged across trials (Fig. 4*A*). Power spectral density differed between the baseline interval (1.5–0 s before stimulus onset), the peristimulus interval (0–1 s after stimulus onset), and the memory interval (2–7.8 s after stimulus onset). Differences were small compared with the range in power across frequencies, and so were recomputed normalized to baseline (prestimulus) power (Fig. 4*B*).

Effects could be described for low, middle, and high frequencies. For low frequencies (theta and alpha bands, 4–8 Hz and 8–16 Hz, respectively), power was elevated in the peristimulus interval compared with baseline. In middle frequencies (beta band, 16–32 Hz), power was highest in the baseline interval, lower in the memory interval, and lowest in the peristimulus interval. For high frequencies (gamma and high-gamma bands, 32–64 and 64–128 Hz, respectively), power was high in the peristimulus interval and marginally lower in the memory interval compared with the baseline interval. Thus, power averaged over the entire memory interval was subtly depressed compared with baseline for frequencies $>\sim$16 Hz.

We next looked at the time course of the power spectral density throughout the trial relative to baseline (Fig. 5*A*). Each band responded at the time of the stimulus. Both theta- and alpha-band power increased sharply with the stimulus, with increases to >50% of their baseline value, then recovered and slightly undershot the baseline (Figs. 5*B*,*C*). Beta-band power decreased during stimulus presentation, dropping to ~25% below baseline level before recovering and slightly overshooting the baseline (Fig. 5*D*). Gamma- and high-gamma-band power increased slightly with the stimulus by ~2 and ~10%, respectively (Figs. 5*E*,*F*).

Surprisingly, beta-, gamma-, and high-gamma-band power gradually decreased throughout the ~7.5 s memory period, dropping below baseline levels after ~3, ~1, and ~5 s, respectively, and continuing to drop for the remainder of the memory period. Linear fits to the power of the three bands throughout the memory period had negative slopes (beta: −0.5%/s, $p = 0.0004$; gamma: 0.5%/s, $p < 10^{-6}$; high-gamma: 0.7%/s, $p < 10^{-6}$; fits exclude the first 2 s of data after stimulus onset to avoid stimulus transients). From 2 to 7.5 s after the stimulus onset, power dropped 7.6% for beta band, 3.3% for gamma band, and 4.3% for high-gamma band. In contrast, theta- and alpha-band power remained close to baseline throughout the memory period. Neither slope was significantly different from zero, though the theta-band slope did border on significance (theta: slope = 0.6%/s, $p = 0.05$; alpha: slope = 0.1%/s, $p = 0.52$). The drop in beta- and gamma-band power is not an artifact of midtrial reward delivery, since the effect can clearly be seen in the 5 and 7.5 s memory trials, in which no rewards were delivered.

Each band exhibited "stimulus-like" responses after midtrial rewards. After these responses, beta and high-gamma power appeared to reset briefly to baseline before immediately dropping below baseline.

LFPs are contralaterally tuned

We next asked whether LFP power reflects the location of the memorized target, i.e., whether LFP power was spatially tuned. For each LFP recording site, we estimated single trial power during the peristimulus and early memory intervals. We fit the data to a von Mises tuning model as a function of target position (see Materials and Methods). Model fits estimated LFP preferred direction (μ), i.e., the stimulus direction that drives the greatest increase or decrease in LFP power, as well as the selectivity, or spread (κ), of this effect.

Tuning differed between frequency bands and across time intervals. During the peristimulus interval, preferred direction distributions for theta, alpha, beta, gamma, and high-gamma bands were clustered contralaterally, with mean preferred directions all within 50 deg of the contralateral direction (Rayleigh's *z*

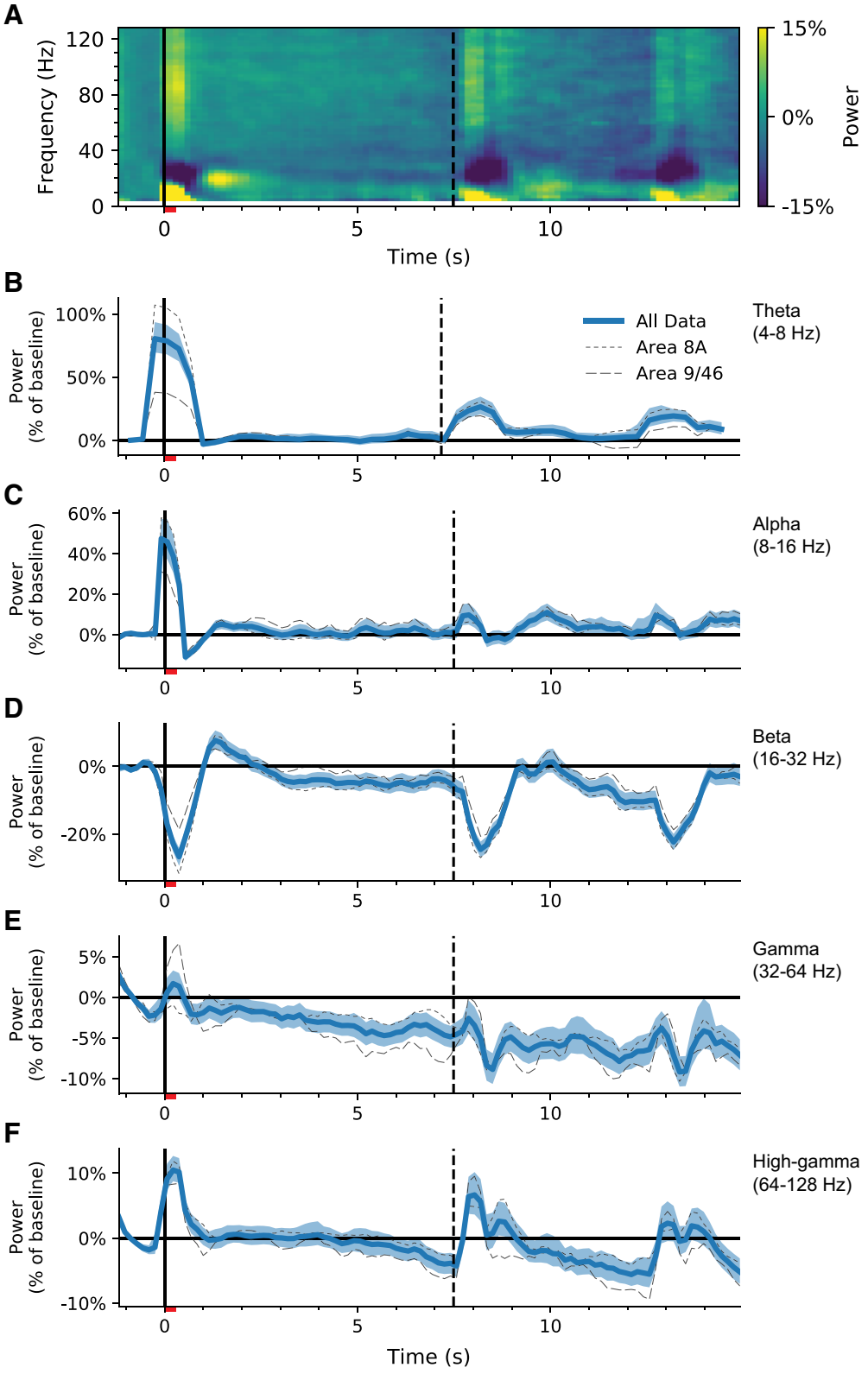

Figure 5. Time course of LFP power. ***A***, Mean percentage modulation of LFP power spectral density from baseline. The stimulus appears at time 0 for 300 ms (*x*-axis, red bar). The vertical dashed line indicates the time of the first midtrial reward. ***B***–***F***, Percentage modulation from baseline of theta- (***B***; 4–8 Hz), alpha- (***C***; 8–16 Hz), beta- (***D***; 16–32 Hz), gamma- (***E***; 32–64 Hz), and high-gamma-band (***F***; 64–128 Hz) power during the task. Power generally increases with the stimulus, with the exception of the beta band, which then climbs above baseline ~1 s later. All bands return to baseline within 1–3 s after stimulus onset. Beta-, gamma-, and high-gamma-band power drop below baseline by 3, 1, and 5 s after stimulus onset, respectively, and continue to decrease through 7.5 s of memory. The solid line is the mean across all recording sites, and the shading is the 95% CI (approximately twice the size of conventional error bars). Thin dashed lines show averages for areas 8A and 9/46, which are very similar to one another and to the global average. Note that responses to stimuli and rewards appear earlier in the theta-band data (***B***) because the spectral analysis window is larger (see Materials and Methods).

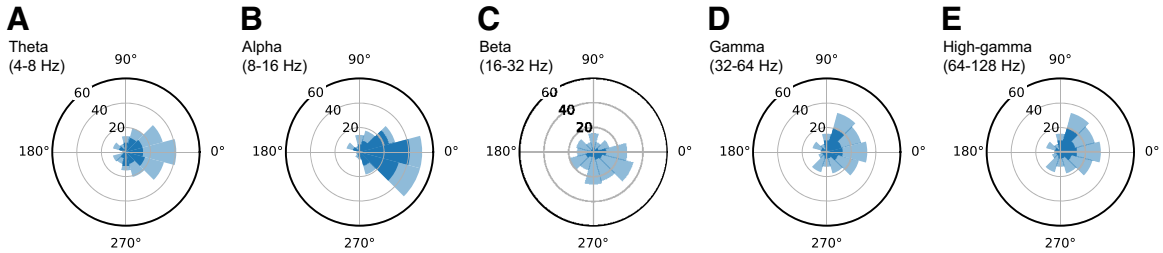

Figure 6. LFP power directional tuning. Distribution of preferred directions of LFP power during the peristimulus interval (0–1 s after stimulus onset). LFP preferred directions were clustered in the contralateral direction (0 deg) for theta (4–8 Hz; ***A***), alpha (8–16 Hz; ***B***), beta (16–32 Hz; ***C***), gamma (32–64 Hz; ***D***), and high-gamma power (64–128 Hz; ***E***). In each plot, dark colors represent sites with significant tuning ($p < 0.05$; *F* test) and light colors represent sites without significant tuning.

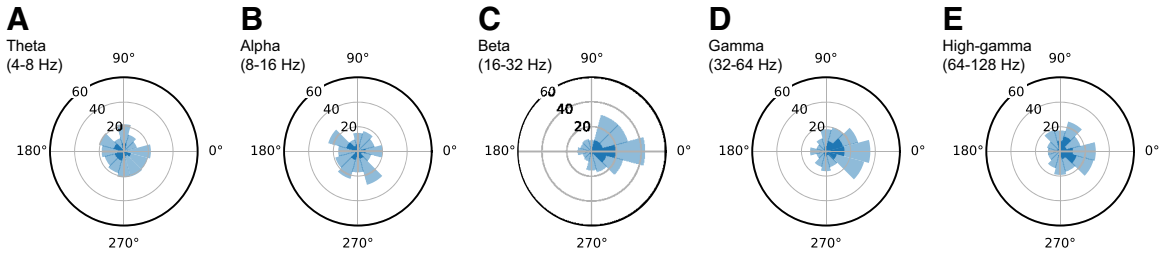

Figure 7. LFP power directional tuning. Distribution of preferred directions of LFP power during the early memory interval (2–5.3 s after stimulus onset) intervals. Theta- (***A***) and alpha-band (***B***) preferred directions became uniformly clustered, whereas beta- (***C***), gamma- (***D***), and high-gamma-band (***E***) preferred directions remained contralaterally clustered. Format as in Figure 6.

tests, $N = 215$, all $p < 10^{-6}$; Fig. 6). Tuning was strongest for the theta and alpha bands, for which 98 and 133 of 215 sites (46 and 62%), respectively, exhibited significant tuning ($p < 0.05$; *F* test). The distribution of mean preferred directions clustered tightly around the contralateral direction: just over half of all sites (theta: 107/215, 50%; alpha: 131/215, 61%) had a preferred direction within 45 deg of the contralateral direction, and almost all tuned sites (theta: 76/98, 78%; alpha: 122/133, 92%) were within 90 deg of the contralateral direction (Figs. 6*A*,*B*). Beta and gamma bands were weakly tuned, with only 47 and 48 individual sites (22% each), respectively, reaching statistical significance, with the majority contralateral (Figs. 6*C*,*D*). Across all sites, tuned and untuned, 131 (61%) showed a beta-band contralateral preference ($p = 0.002$, binomial test) and 146 (68%) showed a gamma-band contralateral preference ($p < 10^{-6}$). High-gamma-band power was moderately tuned and clustered, with 85 sites (40%) reaching significance, and 157 sites (73%) showing a contralateral preference (Fig. 6*E*).

In addition to a preferred target direction, von Mises fits quantify the selectivity of tuning as the spread of the curve (κ). We computed the FWHM (Asher et al., 2007). We only included sites with significant fits. Alpha band had the lowest selectivity, with a median FWHM 91 deg. Theta and high-gamma power had intermediate selectivity, with median FWHM values of 70 and 74 deg, respectively. Beta and gamma power had the greatest selectivity, with median FWHM values of 58 and 54 deg, respectively.

We next assessed tuning during memory. We used an early memory interval, from 2 to 5.3 s after stimulus onset, which allowed us to use every trial in our average (only 2/3 of the data had memory intervals $>\sim$5 s). During memory, tuning weakened for theta and alpha bands (Figs. 7*A*,*B*). Preferred directions were no longer clustered (theta: $z_{(215)} = 0.6$, $p = 0.55$; alpha: $z_{(215)} = 1.7$, $p = 0.18$). Individual sites exhibited significant tuning (theta: 51/215, 24%; alpha: 49/215, 23%), but these subsets were not significantly clustered (theta: $z_{(51)} = 0.29$, $p = 0.06$; alpha: $z_{(49)} = 0.60$, $p = 0.55$). In contrast, beta, gamma, and high-gamma bands remained contralaterally clustered (all $p < 10^{-4}$; Figs. 7*C*–*E*). Both beta and gamma bands had more individually tuned sites during memory compared with the stimulus (beta: 58/215, 27%; gamma: 61/215, 28%), whereas high-gamma band had fewer tuned sites (64/215, 30%).

Tuning selectivity changed from the peristimulus interval to the memory interval. Both theta- and alpha-band selectivities increased, from median FWHM values of 70 and 91 deg to 40 and 41 deg, respectively. Gamma band became less selective, increasing from 54 to 88 deg. Both beta band and high-gamma band roughly maintained their selectivities moving from 58 to 56 deg and from 74 to 68 deg, respectively.

LFP tuning is sustained over memory

We next investigated the time course of LFP tuning and whether tuning waned similarly to absolute power. For this purpose, we defined LFP tuning as the difference in power between contralateral and ipsilateral trials. The appearance of the stimulus sharply increased tuning in all but the beta band (Fig. 8*A*), with particularly high increases in theta and alpha. Within $\sim$1 s of stimulus presentation, theta and alpha tuning disappeared, high-gamma tuning dropped dramatically, and beta tuning began to ramp up. Figures 8, *B* and *C*, show the time course of theta and alpha tuning, respectively. Here we normalized the tuning (the difference in power for trials with contralateral versus ipsilateral stimuli) by expressing it as a percentage of the mean baseline power. Theta tuning rose markedly with the stimulus, peaking at $\sim$120% of baseline power (i.e., power on contralateral trials exceeded power on ipsilateral trials by 1.2 times the average baseline power), returning to zero (no difference in power on contralateral compared with ipsilateral trials) within $\sim$1 s, and staying at zero for the rest of the memory period [2–7.8 s; bootstrap 95% CI, (−3.0%, 1.8%)]. Similarly, alpha tuning rose to $\sim$70% with the stimulus, returned to zero within 1 s, and was untuned during memory [bootstrap 95% CI, (−0.8%, 2.8%)].

In contrast, beta, gamma, and high-gamma power showed clear and sustained memory-period tuning (Figs. 6*D*–*F*). Beta tuning ramped up during the stimulus interval. Within $\sim$1 s, the

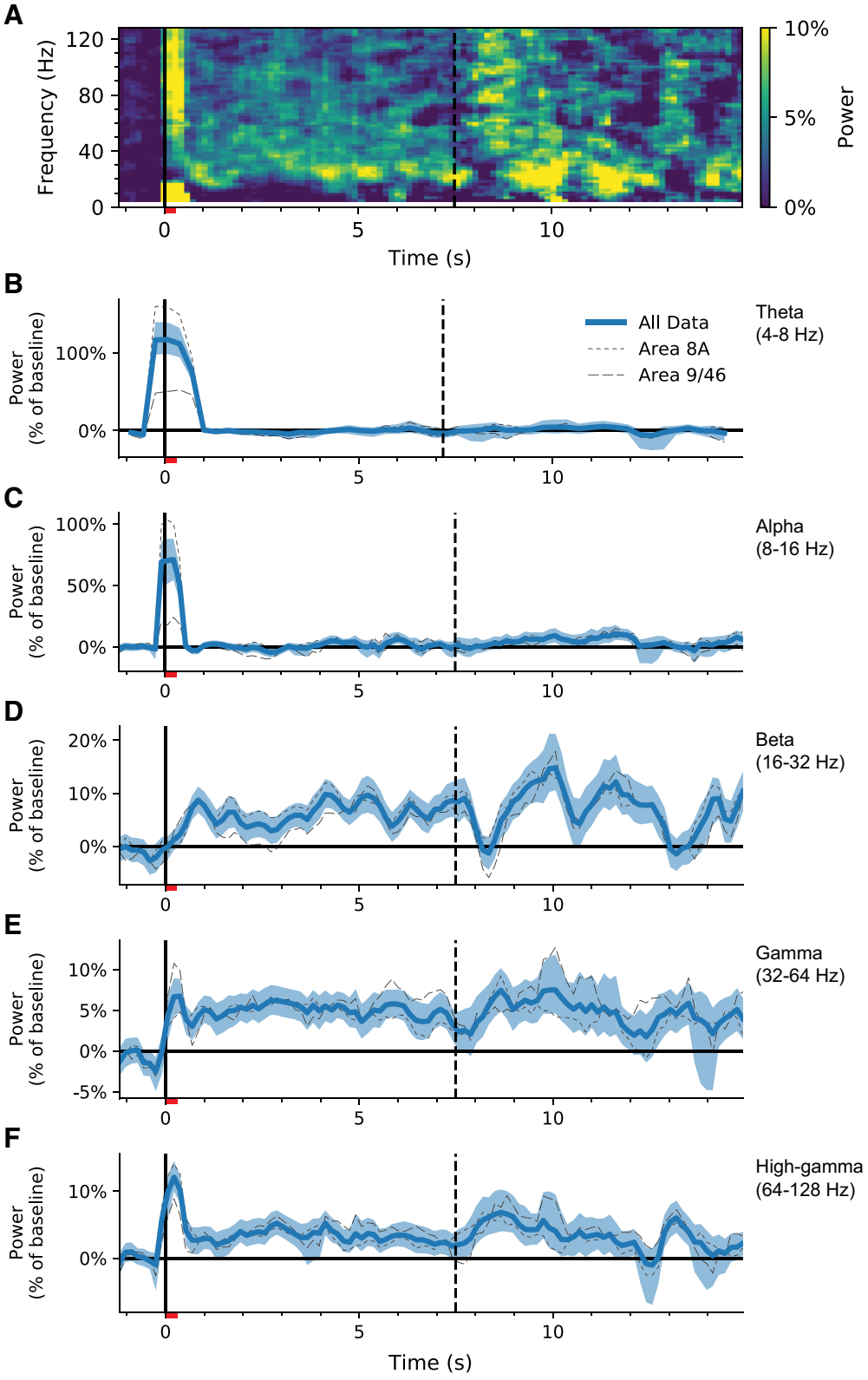

Figure 8. Time course of LFP power tuning. The difference in LFP power between contralateral and ipsilateral stimuli; format as in Figure 5. ***A***, Mean tuning of LFP power spectral density as a percentage of absolute baseline power spectral density. ***B***–***F***, Tuning of individual bands as a percentage of absolute baseline power. All but beta are tuned for the stimulus. Within ~1 s, theta (***B***) and alpha (***C***) become untuned, whereas gamma (***E***) and high-gamma bands (***F***) remain tuned throughout 7.5 s of memory. Beta-band tuning (***D***) ramps up over ~1 s and persists for the remainder of the ~15 s memory period. Both area 8A and area 9/46 resembled the global averages when considered separately (thin dashed lines). Shaded region corresponds to the 95% CI, which is approximately twice the size of conventional error bars.

LFP power modulation for a contralateral target was ~5–10% greater than for an ipsilateral target. Tuning persisted for the entire ~7.5 s memory period, with a mean value of 6.6% [bootstrap 95% CI (5.3%, 7.9%)]. Gamma tuning was also sustained throughout the memory period, with a mean value of 5.0% [bootstrap 95% CI (4.0%, 6.2%)]. High-gamma tuning dropped after its stimulus response but settled to a sustained mean value of 3.4% [bootstrap 95% CI (2.2%, 4.8%)] for the remainder of the memory interval. Thus, all bands exhibited tuning, with frequencies >~16 Hz sustaining their tuning over the entire memory interval.

LFP power reflects memory accuracy

We assessed whether LFP power reflected memory accuracy. We performed a median split of successful trials from each recording session according to the absolute saccadic error. We compared both absolute LFP power and LFP laterality tuning during the memory interval (2–7.8 s after stimulus onset) for the three bands with memory period effects: beta, gamma, and high-gamma. Beta-band power was, on average, 1.5% lower [bootstrap 95% CI (0.6%, 2.5%)] for accurate trials than for inaccurate trials. To protect against multiple comparisons, we computed a bootstrap 99.17% CI (Bonferroni correction for 6 comparisons), which was still significant (0.2%, 2.8%). Thus, greater mnemonic accuracy was linked to lower LFP power. Both gamma and high-gamma power were also lower for accurate trials than for inaccurate trials (gamma, 0.3% lower; high-gamma, 0.5% lower), but these effects were not significant even with an uncorrected test (bootstrap 95% CIs included 0). None of the three bands exhibited a significant difference in laterality tuning as a function of accuracy.

Discussion

Neurons in the prefrontal cortex show sustained increases in activity during memory retention that are tuned for target location (Funahashi et al., 1989; Wimmer et al., 2014). We reasoned that this activity may be associated with increased neuronal synchronization at the circuit- or ensemble-level and that this synchronization would present as either a memory-evoked potential or memory-related increase in LFP power. Previous work has shown that holding memories for a few seconds is associated with evoked responses in the LFP (Monosov et al., 2008) and power modulations in theta (Jensen and Tesche, 2002; Hsieh et al., 2011), alpha (Jensen et al., 2002; Hsieh et al., 2011), beta (Roberts et al., 2013; Kornblith et al., 2016), and gamma frequencies (Pesaran et al., 2002; Howard et al., 2003; Roberts et al., 2013; Kornblith et al., 2016). In this study, we considered longer memory periods and found that although beta, gamma, and high-gamma power remain tuned for 7.5 s of memory, absolute power in these bands drops continuously over this period.

We observed an evoked (phase-synchronous) potential at the time of the stimulus that lasted for no more than 1 s. This could reflect a response to the stimulus per se, or might also reflect memory encoding (Monosov et al., 2008). In contrast, LFP power, like spiking activity, exhibited a spatially tuned response that, for some frequencies, lasted for the full duration of the memory period (Fig. 8). Theta- and alpha-band tuning lasted for <1 s after stimulus onset. Beta-band tuning ramped up over the first second and then stayed constant for the remainder of the 7.5 s memory period. Both gamma- and high-gamma-band tuning appeared immediately and was sustained, like beta, for the duration of the memory period. These data suggest that theta and alpha bands may reflect sensory, attentional, or encoding processes, beta band may reflect memory and storage processes, and gamma and high-gamma bands may reflect some combination of those processes.

There was a second unexpected effect of memory on LFP; a slow drop in absolute power below baseline (Fig. 5). Initially, LFP power in all bands increased abruptly with stimulus presentation, with the exception of beta-band power, which decreased. This is consistent with previous observations that gamma-band power resembles firing rate (Pesaran et al., 2002), whereas beta changes inversely with gamma (Kornblith et al., 2016). However, after these transient changes, LFP power >~16 Hz fell, returning to baseline within ~5 s and falling below baseline over the remainder of the 7.5 s memory interval. This gradual drop in absolute LFP power may relate to memory processing in a number of ways. One possibility is that absolute LFP power reflects memory robustness. LFP power tracks with decay in task performance, i.e., precision (compare Figs. 1*C*,*D*, 5*D*–*F*). However, precision cannot fully explain the results: even if we expect a drop in LFP power with decreasing precision, we would not expect power to drop below baseline. Furthermore, we would also expect a decay in LFP tuning, which instead remains persistent.

A second possible way that the drop in power may relate to memory processing comes from modeling work by Compte et al. (2000), who demonstrate that in a neural attractor network, synchronization can lead to an overall instability that is not compatible with a stable memory-coding state. In contrast, asynchronous networks can maintain memory coding for durations on the order of ~10 s. Thus, frontal memory networks may desynchronize to preserve memory states. In this scenario, the gradual drop in LFP power may reflect overall desynchronization, whereas the tuned increase in LFP power reflects the maintenance of the memory.

Further support of this hypothesis comes from the study of synaptic dynamics. One way to promote asynchrony in a memory network is for excitatory dynamics to be slower than inhibitory dynamics. NMDA and AMPA channels are the two major excitatory channels in the CNS, whereas GABA channels are the major inhibitory channels. Compared with GABA channels, NMDA channels are slower, whereas AMPA channels are faster. Biorealistic models suggest that a higher ratio of NMDA to AMPA channels, i.e., slower excitatory dynamics, promotes network desynchronization and, thus, memory state stability (Compte et al., 2000). In humans, dorsolateral prefrontal cortex has a greater expression of NMDA channels than do primary visual, motor, or parietal cortex (Scherzer et al., 1998), consistent with slow NMDA dynamics playing a role in memory. In primates performing a memory task, blockade of NMDA channels with NMDA channel antagonists reduces the memory related activity in area 9/46, whereas administration of NMDA channel agonists increases the activity (Wang et al., 2013). Furthermore, rodent studies have shown that blockade or removal of NMDA channels can alter ensemble synchronization, by increasing LFP gamma-band power or by increasing noise correlation between neurons (Carlén et al., 2012; Herrero et al., 2013; Kealy et al., 2017), which is consistent with NMDA playing a role in ensemble desynchronization.

In support of this hypothesis, we found that beta-band power was lower for accurate trials compared with inaccurate trials. Gamma and high-gamma power, showed a similar trend, but the effects were statistically insignificant. In line with our data, another study demonstrated that beta-band synchrony (both within and across area) drops during memory (Kornblith et al., 2016). In summary, our results demonstrate that accurate mnemonic behavior is linked to lower LFP power. In turn, these data

provide correlative evidence that supports a role of frontal neuronal desynchronization in memory retention and robustness.

Other work has reported memory effects that appear in single trials as isolated beta- and gamma-band bursts (Lundqvist et al., 2016). Our results also show "speckling" in both time and frequency (Figs. 5, 8), but our data are averaged over time and sites. We believe that, in our data, the specking is the result of low-pass filtering (in time and frequency) the signal and then color-coding it so that small fluctuations are accentuated. We do not have a high enough signal-to-noise ratio to judge with confidence the pattern of responses on individual trials.

More generally, our findings add to a growing literature that LFPs are rich signals that reflect cognitive processing, including memory. As in our data, effects are not limited to a single band, but rather can be seen across the spectrum from theta to high-gamma (Markowitz et al., 2011, 2015; Kornblith et al., 2016). LFPs do not necessarily reflect the same information as local neurons. Areas with weak topography can have information smeared away in spatially integrative signals such as LFPs (Leavitt et al., 2017). LFPs can also reflect subthreshold cellular activity that do not result in spikes, e.g., though spikes in MT do not reflect memorized information, LFPs do (Mendoza-Halliday et al., 2014). LFPs provide a means to investigate cortical circuit function and organization that compliments unit recording.

Our data provide insight regarding an ongoing debate between rate codes and temporal code as the substrate of memory. Much evidence has demonstrated that oscillatory cortical activity is modulated by memory and other cognitive processes (Pesaran et al., 2002; Kornblith et al., 2016). Other studies have suggested that the timing of spikes with relation to such oscillations can convey information beyond the firing rate alone (O'Keefe and Recce, 1993; Siegel et al., 2009). Our data suggest that oscillatory activity by itself is likely not a substrate of memory. Though our data demonstrate that oscillatory activity (LFP power) exhibits tuning, a model emphasizing spike timing with relation to oscillatory activity would predict that oscillatory activity would be prominent during memory and would correlate with accuracy. Instead, our data demonstrate that LFP power drops below baseline and is lower in accurate trials. Tuning may be an epiphenomenon of a rate code in the circuit, rather than a direct substrate.

References

Asher I, Stark E, Abeles M, Prut Y (2007) Comparison of direction and object selectivity of local field potentials and single units in macaque posterior parietal cortex during prehension. J Neurophysiol 97:3684–3695. CrossRef Medline

Buzsáki G, Wang XJ (2012) Mechanisms of gamma oscillations. Annu Rev Neurosci 35:203–225. CrossRef Medline

Buzsáki G, Anastassiou CA, Koch C (2012) The origin of extracellular fields and currents: EEG, ECoG, LFP and spikes. Nat Rev Neurosci 13:407–420. CrossRef Medline

Carlén M, Meletis K, Siegle JH, Cardin JA, Futai K, Vierling-Claassen D, Rühlmann C, Jones SR, Deisseroth K, Sheng M, Moore CI, Tsai LH (2012) A critical role for NMDA receptors in parvalbumin interneurons for gamma rhythm induction and behavior. Mol Psychiatry 17:537–548. CrossRef Medline

Cohen MR, Kohn A (2011) Measuring and interpreting neuronal correlations. Nat Neurosci 14:811–819. CrossRef Medline

Compte A, Brunel N, Goldman-Rakic PS, Wang XJ (2000) Synaptic mechanisms and network dynamics underlying spatial working memory in a cortical network model. Cereb Cortex 10:910–923. CrossRef Medline

DiCiccio TJ, Efron B (1996) Bootstrap confidence intervals. Stat Sci 11:189–228. CrossRef

Funahashi S, Bruce CJ, Goldman-Rakic PS (1989) Mnemonic coding of visual space in the monkey's dorsolateral prefrontal cortex. J Neurophysiol 61:331–349. CrossRef Medline

Herrero JL, Gieselmann MA, Sanayei M, Thiele A (2013) Attention-induced variance and noise correlation reduction in macaque v1 is mediated by NMDA receptors. Neuron 78:729–739. CrossRef Medline

Howard MW, Rizzuto DS, Caplan JB, Madsen JR, Lisman J, Aschenbrenner-Scheibe R, Schulze-Bonhage A, Kahana MJ (2003) Gamma oscillations correlate with working memory load in humans. Cereb Cortex 13:1369–1374. CrossRef Medline

Hsieh LT, Ekstrom AD, Ranganath C (2011) Neural oscillations associated with item and temporal order maintenance in working memory. J Neurosci 31:10803–10810. CrossRef Medline

Jensen O, Tesche CD (2002) Frontal theta activity in humans increases with memory load in a working memory task. Eur J Neurosci 15:1395–1399. CrossRef Medline

Jensen O, Gelfand J, Kounios J, Lisman JE (2002) Oscillations in the alpha band (9–12 Hz) increase with memory load during retention in a short-term memory task. Cereb Cortex 12:877–882 CrossRef Medline

Kealy J, Commins S, Lowry JP (2017) The effect of NMDA-R antagonism on simultaneously acquired local field potentials and tissue oxygen levels in the brains of freely-moving rats. Neuropharmacology 116:343–350. CrossRef Medline

Kornblith S, Buschman TJ, Miller EK (2016) Stimulus load and oscillatory activity in higher cortex. Cereb Cortex 26:3772–3784. CrossRef Medline

Leavitt ML, Mendoza-Halliday D, Martinez-Trujillo JC (2017) Sustained activity encoding working memories. Trends Neurosci 40:328–346. CrossRef Medline

Lundqvist M, Rose J, Herman P, Brincat SL, Buschman TJ, Miller EK (2016) Gamma and beta bursts underlie working memory. Neuron 90:152–164. CrossRef Medline

Markowitz DA, Wong YT, Gray CM, Pesaran B (2011) Optimizing the decoding of movement goals from local field potentials in macaque cortex. J Neurosci 31:18412–18422. CrossRef Medline

Markowitz DA, Curtis CE, Pesaran B (2015) Multiple component networks support working memory in prefrontal cortex. Proc Natl Acad Sci U S A 112:11084–11089. CrossRef Medline

Mendoza-Halliday D, Torres S, Martinez-Trujillo JC (2014) Sharp emergence of feature-selective sustained activity along the dorsal visual pathway. Nat Neurosci 17:1255–1262. CrossRef Medline

Monosov IE, Trageser JC, Thompson KG (2008) Measurements of simultaneously recorded spiking activity and local field potentials suggest that spatial selection emerges in the frontal eye field. Neuron 57:614–625. CrossRef Medline

O'Keefe J, Recce ML (1993) Phase relationship between hippocampal place units and the EEG theta rhythm. Hippocampus 3:317–330. CrossRef Medline

Percival DB, Walden AT (1993) Spectral analysis for physical applications. In: Spectral analysis for physical applications: multitaper and conventional univeriate techniques, pp 331–377. Cambridge, UK: Cambridge UP.

Pesaran B, Pezaris JS, Sahani M, Mitra PP, Andersen RA (2002) Temporal structure in neuronal activity during working memory in macaque parietal cortex. Nat Neurosci 5:805–811. CrossRef Medline

Petrides M, Tomaiuolo F, Yeterian EH, Pandya DN (2012) The prefrontal cortex: comparative architectonic organization in the human and the macaque monkey brains. Cortex 48:46–57. CrossRef Medline

Roberts BM, Hsieh LT, Ranganath C (2013) Oscillatory activity during maintenance of spatial and temporal information in working memory. Neuropsychologia 51:349–357. CrossRef Medline

Scherzer CR, Landwehrmeyer GB, Kerner JA, Counihan TJ, Kosinski CM, Standaert DG, Daggett LP, Veliçelebi G, Penney JB, Young AB (1998) Expression of *N*-methyl-D-aspartate receptor subunit mRNAs in the human brain: hippocampus and cortex. J Comp Neurol 390:75–90. CrossRef Medline

Siegel M, Warden MR, Miller EK (2009) Phase-dependent neuronal coding of objects in short-term memory. Proc Natl Acad Sci U S A 106:21341–21346. CrossRef Medline

Wang M, Yang Y, Wang CJ, Gamo NJ, Jin LE, Mazer JA, Morrison JH, Wang XJ, Arnsten AF (2013) NMDA receptors subserve persistent neuronal firing during working memory in dorsolateral prefrontal cortex. Neuron 77:736–749. CrossRef Medline

Wimmer K, Nykamp DQ, Constantinidis C, Compte A (2014) Bump attractor dynamics in prefrontal cortex explains behavioral precision in spatial working memory. Nat Neurosci 17:431–439. CrossRef Medline

Zar JH (1974) Circular distributions: hypothesis testing. In: Biostatistical Analysis, Ed 4, pp 616–663. Upper Saddle River, NJ: Pearson.